Optimum design of photoresist thickness for 90-nm critical dimension based on ArF laser lithography*

Chen De-Liang(陈德良), Cao Yi-Ping(曹益平)†, Huang Zhen-Fen(黄振芬),
Lu Xi(卢 熙), and Zhai Ai-Ping(翟爱平)

Department of Opto-Electronics, Sichuan University, Chengdu 610065, *China*

(Received 10 December 2011; revised manuscript received 20 January 2012)

In this work, a 90-nm critical dimension (CD) technological process in an ArF laser lithography system is simulated, and the swing curves of the CD linewidth changing with photoresist thickness are obtained in the absence and presence of bottom antireflection coating (BARC). By analysing the simulation result, it can be found that in the absence of BARC the CD swing curve effect is much bigger than that in the presence of BARC. So, the BARC should be needed for the 90-nm CD manufacture. The optimum resist thickness for 90-nm CD in the presence of BARC is obtained, and the optimizing process in this work can be used for reference in practice.

Keywords: lithography, optimization, photoresist thichness, critical dimension, swing curve

PACS: 42.25.Bs, 42.25.Kb, 42.30.Kq, 42.70.Gi **DOI:** 10.1088/1674-1056/21/8/084201

1. Introduction

In lithography, because of the reflection at the interface between photoresist and substrate, there has been observed the standing wave effect[1−3] and the swing curve effect in the photoresist.[4,5] Upon reflection at the interface between photoresist and substrate a phase shift occurs in the light reflected back toward the photoresist surface. The path length that the light travels through the resist determines its phase and whether the interference will be constructive or destructive. Interference between the outgoing and incoming light waves, owing to a phase difference between them, will result in a standing wave and swing curve. This phenomenon is also called the thin-film interference effect.[5] With the trend toward smaller feature size, it is more and more important to control the resist thickness and uniformity to a tight tolerance in order to minimize thin film interference effects on the critical dimensions (CDs). The method of controlling the resist thickness was extensively studied, and the traditional method is to deposit bottom antireflection coating (BARC) on the silicon surface for reducing the reflectivity.[6−12] However depositing BARC cannot perfectly reduce the effect of the reflectivity, and the swing curve effect cannot be avoided and it still exists. In addition, depositing BARC can increase the technological process (the depositing process and the removing process) and the cost. So we should first ascertain whether the BARC is needed for the CD manufacture, and then obtain the optimal resist thickness.

In the present paper, we use the Hopkins's partial coherent image theory,[13,14] Dill's expose model,[15] post-exposure bake model,[16] and Mack's develop model[17] for building the lithography simulation model and realize this lithography simulation model with the Matlab program. Using this model, the 90-nm CD's technological process based on ArF laser lithography system is simulated. According to the simulation result, we find that in the absence of BARC the effect of the CD swing curve is very serious. So, the BARC should be needed for the 90-nm CD manufacture based on ArF laser lithography and the optimal resist thickness for 90-nm CD in the presence of BARC is obtained at a certain expose dose.

2. Simulation model of lithography

Lithography simulation relies on models from two fields of science; one is optics to model the formation of

*Project supported by the National Special Program of China (Grant No. 2009ZX02204-008) and the National Basic Research Program of China (Grant No. 2007AA01Z333).

†Corresponding author. E-mail: ypcao@scu.edu.cn

© 2012 Chinese Physical Society and IOP Publishing Ltd

the aerial image, and the other is chemistry to model the formation of the latent image in the resist.

The optical model used for calculating the aerial image is shown in Fig. 1, which is accepted by most commercial simulation softwares. As shown in Fig. 1, the actual source and the condenser system are replaced by the equivalent effective source having an irradiance distribution of $r(x_0, y_0)$ where (x_0, y_0) refers to the spatial coordinate of the normalized coherent factor (sigma) on the effective source plane, and the mask is considered to have a digital transmission function given by

$$t(x_1, y_1) = \begin{cases} 1, & \text{in clear areas,} \\ 0, & \text{in opaque areas,} \end{cases} \tag{1}$$

where (x_1, y_1) denotes the mask plane. According to the discussion of coherent imaging in Hopkins's paper[13,14], if the point source is assumed to be on-axis such that $(x_0, y_0) = (0, 0)$, after the point source light is diffracted on the mask plane, the spectrum of the mask is described by the Fraunhofer diffraction integral

$$\varepsilon(f_x, f_y) = \int_{-\infty}^{+\infty} \int_{-\infty}^{+\infty} t(x_1, y_1) \times \mathrm{e}^{-2\pi \mathrm{j}(f_x x_1 + f_y y_1)} \mathrm{d}x_1 \mathrm{d}y_1, \tag{2}$$

where f_x and f_y are the spatial frequencies of the diffraction pattern defined as

$$f_x = \frac{x'}{z_0 \lambda} \quad \text{and} \quad f_y = \frac{y'}{z_0 \lambda}, \tag{3}$$

$\varepsilon(f_x, f_y)$ is the Fourier transform of the mask pattern, $(x',\ y')$ denotes the aperture plane, (x, y) denotes the wafer plane, z_0 is the distance between the mask plane and the first lens surface of the projection system, and λ is the wavelength of the source light. For a general source point where $(x_0, y_0) \neq (0, 0)$, we can make the approximation that the optical system is shift-invariant such that the spectrum of the mask, owing to the source point, can be described by

$$\varepsilon'(f_x, f_y) = \varepsilon(f_x - x_0, f_y - y_0). \tag{4}$$

The image on the wafer plane arising from the source point can be described by

$$I'(x, y) = \left| FT^{-1} \left\{ \varepsilon'(f_x, f_y) P(f_x, f_y) \right\} \right|^2, \tag{5}$$

and

$$P(f_x, f_y) = \begin{cases} 1, & \text{if } \sqrt{f_x^2 + f_y^2} < \dfrac{NA}{\lambda}, \\ 0, & \text{if } \sqrt{f_x^2 + f_y^2} > \dfrac{NA}{\lambda}, \end{cases} \tag{6}$$

where $P(f_x, f_y)$ denotes the pupil function of the optical system, NA means the numerical aperture, and FT^{-1} refers to inverse Fourier transform. Since, by definition, the effective source is equivalent to a self-luminous source, the total irradiance at wafer plane can be obtained by integrating over the entire effective source, and can be written as

$$\begin{aligned} I(x, y) &= \iint_{\Sigma} r(x_0, y_0) \left| FT^{-1} \left\{ \varepsilon'(f_x, f_y) P(f_x, f_y) \right\} \right|^2 \\ &\quad \times \mathrm{d}x_0 \mathrm{d}y_0 \\ &= \iint_{\Sigma} r(x_0, y_0) \left| FT^{-1} \{ \varepsilon(f_x - x_0, f_y - y_0) \right. \\ &\quad \left. \times P(f_x, f_y) \} \right|^2 \mathrm{d}x_0 \mathrm{d}y_0, \end{aligned} \tag{7}$$

and,

$$r(x_0, y_0) = \begin{cases} 0, & \text{if} \sqrt{x_0^2 + y_0^2} < \sigma_1, \\ 1, & \text{if } \sigma_1 < \sqrt{x_0^2 + y_0^2} < \sigma_2, \\ 0, & \text{if } \sigma_2 < \sqrt{x_0^2 + y_0^2}, \end{cases} \tag{8}$$

where $r(x_0, y_0)$ is the annular effective source; σ_1 and σ_2 are the inner coherent factor and the outer coherent factor respectively. Equation (7) is the principle relation of a generalized Abbe theory, where the image formation under partially coherent illumination of the object is accounted for by a combination of coherent imaging processes for perpendicular and obliquely incident illuminating plane waves on the object. Since only the image irradiance is of interest, it can be determined without use of the coherence theory. For the computation, the whole source is divided into a number of luminous point sources considering the imaging due to each source acting as an independent coherent image formation process. The contributions from point sources do not interfere, so the net image irradiance is the sum of the irradiance from each source point.

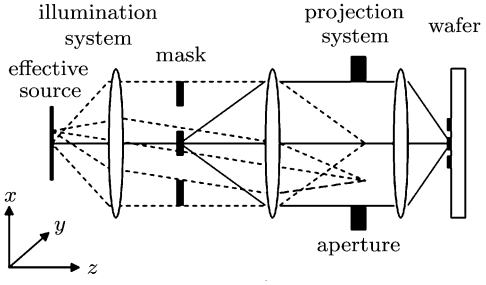


Fig. 1. Optics model for aerial image.

The chemistry model is composed of the exposure model, post exposure bake model, and development model. In this work, the Dill's exposure model is adopted and defined as

$$\frac{\partial I(x,z)}{\partial z} = -\left[A \cdot M(x,z,t) + B\right] \cdot I(x,z),$$
$$\frac{\partial M(x,z,t)}{\partial t} = -C \cdot I(x,z) \cdot M(x,z,t). \tag{9}$$

Here, M is the normalized PAC (photo-active compound) concentration function relating to its pre-exposure value at any position and any time of exposure: in the case of non-exposure, $M = 1$ and $t = 0$, and in the case of full exposure, $M = 0$ and t is equal to full exposure time. A, B, and C are the parameters of Dill's model, and can be measured experimentally. $I(x,z)$ is the two-dimensional relative intensity distribution of light into the photoresist considering the standing wave effect,[18] and can be given by

$$I(x,z) = I(x)\frac{\mathrm{Re}(n_2)}{\mathrm{Re}(n_1)}\left|\frac{\tau_{12}\left\{\exp\left[2\pi \mathrm{j}\mathrm{Re}(n_2)z/\lambda\right] + \rho_{23}\tau_D^2 \exp\left[-2\pi \mathrm{j}\mathrm{Re}(n_2)z/\lambda\right]\right\}}{1+\rho_{12}\rho_{23}\tau_D^2}\right|^2,$$
$$\rho_{12} = \frac{n_1 - n_2}{n_1 + n_2}, \quad \rho_{23} = \frac{n_2 - n_3}{n_2 + n_3}, \quad \tau_{12} = \frac{2n_1}{n_1 + n_2}, \quad \tau_D = \exp\left[\frac{2\pi \mathrm{j}\mathrm{Re}(n_2)D}{\lambda}\right], \tag{10}$$

where ρ_{12} and ρ_{23} are the reflection coefficients; n_1, n_2, and n_3 are the complex refractive indexes of air, resist, and substrate respectively; τ_{12} is the transmission coefficient; D is the resist thickness; τ_D is the internal transmittance of the resist; Re denotes the selecting of the real part. Equations (9) are coupled equations which can be solved simultaneously by resist simulators.

The post exposure bake model can be given by

$$\frac{\mathrm{d}M}{\mathrm{d}t} = \nabla \cdot (D_1 \nabla M), \tag{11}$$

and

$$D_1 = D_o \, \mathrm{e}^{(-D_E/kT)}, \tag{12}$$

where M is the normalized PAC concentration which can be calculated by solving two-dimensional diffusion according to Eqs. (11) and (12), and t is the bake time, and D_1 is the diffusion coefficient with the parameters of D_o and D_E.

The Mack's develop model is selected, and can be given by

$$R(x,z) = R_{\max} \cdot \frac{(a+1)(1-M(x,z))^n}{a + (1-M(x,z))^n} + R_{\min}, \tag{13}$$
$$a = \frac{n+1}{n-1} \cdot (1 - M_{\mathrm{th}})^n, \tag{14}$$

where $R(x,z)$ is the development rate of the photoresist, $M(x,z)$ is the normalized PAC concentration distribution into the photoresist after exposure and bake, n is a selectivity parameter describing the sensitivity of the developer to the exposed photoresist, M_{th} is the threshold normalized PAC concentration, $R_{\max}$ is the development rate of a completely exposed resist, and $R_{\min}$ is the totally unexposed resist. The Mack's develop model can be realized by the Cellular Automata algorithm.[19]

3. Simulation process

According to the above model, we simulate the lithography technique for 90-nm CD. The parameters of each simulation model are given in Table 1, and the parameters for 193-nm laser lithography are set according to Refs. [18] and [20].

In order to verify the effect of the anti-reflectivity of BARC, we compute the total reflectivity in the presence and absence of BARC. Because the thickness of BARC also affects the total reflectivity, we should first optimize the thickness of BARC. Figure 2 shows the reflectivity varying with the thickness of the chosen BARC. From Fig. 2, we find that the second minimum reflectivity corresponds to the optimal thickness of BARC. So we can choose this thickness. At this thickness, the contribution to the total reflectivity can be ignored. After ignoring the effect of the BARC thickness, the reflectivity computational formula can be given by[20]

$$R = \frac{|\rho_{12}|^2 + |\rho_{23}|^2 \, \mathrm{e}^{-\alpha 2D} + 2\,|\rho_{12}\rho_{23}|\, \mathrm{e}^{-\alpha D}\cos(4\pi \mathrm{Re}(n_2)D/\lambda - \phi_{12} + \phi_{23})}{1 + |\rho_{12}\rho_{23}|^2 \, \mathrm{e}^{-\alpha 2D} + 2\,|\rho_{12}\rho_{23}|\, \mathrm{e}^{-\alpha D}\cos(4\pi \mathrm{Re}(n_2)D/\lambda + \phi_{12} + \phi_{23})},$$
$$\alpha = \frac{2\pi\kappa}{\lambda}, \quad \phi_{12} = -\mathrm{i}(\ln\rho_{12} - \ln|\rho_{12}|), \quad \phi_{23} = -\mathrm{i}(\ln\rho_{23} - \ln|\rho_{23}|), \tag{15}$$

where R denotes the reflectivity, α is the absorption coefficient of the resist, and κ is the imaginary part of n_2.

Table 1. Parameters of lithography simulation.

Parameter	Value
Wavelength/nm	193
NA	0.75
Illumination	annular 0.85/0.55 (out/inter sigma)
Substrate	BARC (complex refractive index: 1.82 + i0.34)
	silicon (complex refractive index: 0.883 + i2.778)
Resist	complex refractive index: 1.71 + i0.018
Air	complex refractive index: 1
Dill's exposure model	$A = 0$ μm^{-1}, $B = 1.20$ μm^{-1}, $C = 0.05$ cm^2/mJ, expose dose = 25.5 mJ/cm^2
Post exposed bake	$D_o = 7.55 \times 10^{-13}$, $D_E = 3.34 \times 10^{-2}$, time = 60 s, temperature = 125 °C
Mack's develop model	$R_{\max} = 0.1$ μm/s, $R_{\min} = 0.0001$ μm/s, $M_{\text{th}} = 0.5$, $n = 8$, time = 60 s, steps = 6

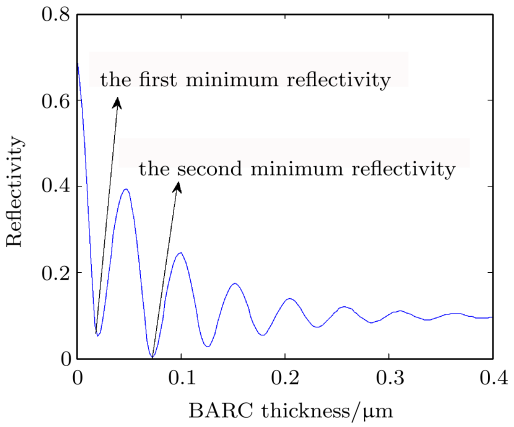


Fig. 2. Reflectivity varying with the thickness of the chosen BARC.

As shown in Fig. 3, the reflectivity in the absence of BARC is far larger than the reflectivity in the presence of BARC, and the swing curve effect is also very obvious. Adding BARC can reduce the reflectivity and the swing curve effect, but cannot change the period of the swing curve.

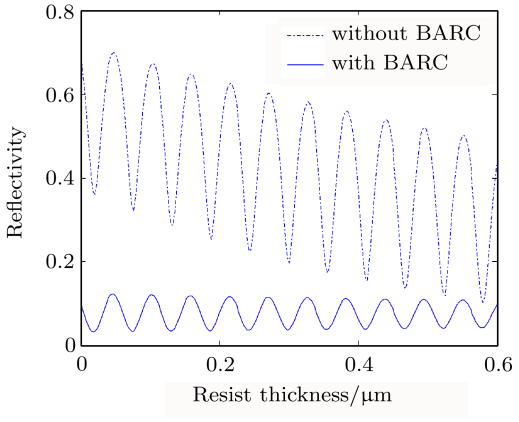


Fig. 3. Swing curve of reflectivity.

Using the parameters in Table 1, we simulate the changes of the 90-nm CD with resist thickness in the presence of and the absence of BARC separately. The deposited resist thickness varies from 0.1 μm to 0.6 μm in steps of 0.01 μm. Figure 4 shows the simulation results under the two conditions. From Fig. 4, it can be found that the swing amplitude of the CD linewidth in

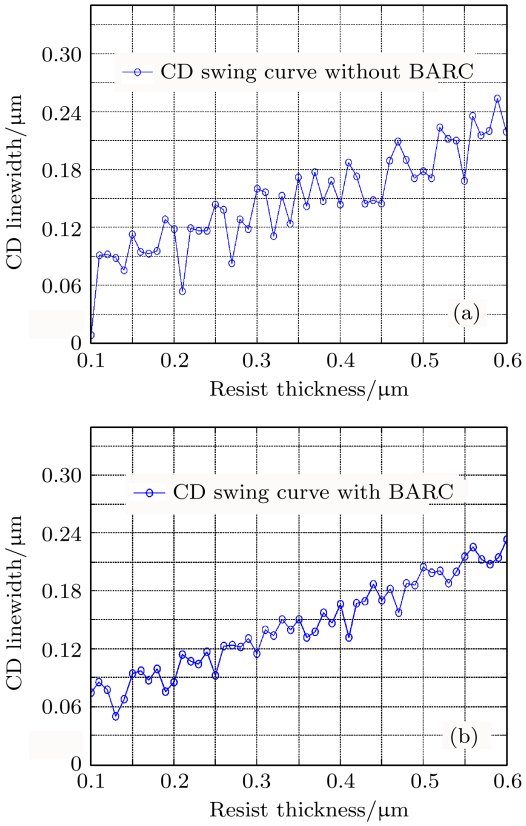


Fig. 4. Swing curves of 90-nm CD linewidth versus resist thickness in the absence (a) and presence (b) of BARC.

the presence of BARC is smaller than that in the absence of BARC. As shown in Fig. 4(a), when the resist

thickness is less than 0.11 μm, the CD is over-exposed; when the resist thickness is greater than 0.28 μm, the CD is under-exposed. So the optimal resist thickness in the absence of BARC should be chosen to be between 0.11 μm to 0.28 μm. Furthermore, we find that when the resist thickness is between 0.11 μm and 0.14 μm, the swing amplitude of the CD linewidth is small, and the CD linewidth is closer to the ideal value. So the range of the optimal resist thickness is further shrunk to the range from 0.11 μm to 0.14 μm. According to the similar choosing rules, the optimized resist thickness for 90-nm CD in the presence of BARC is found to be between 0.15 μm to 0.18 μm.

In order to obtain further accurate resist thickness, the adding step of resist thickness in simulation is set to be 0.0025 μm. At this increasing step, the swing curves of the CD linewidth within the optimized resist thickness ranges of the two conditions are obtained separately by simulation, and the results are shown in Fig. 5. As shown in Fig. 5, the swing amplitude of the CD linewidth in the presence of BARC is less than 10% within the optimal thickness range from 0.15 μm to 0.18 μm. So, if the deposit resist thickness is within the range from 0.15 μm to 0.18 μm in the presence of BARC, the obtained CD linewidth will be accurate.

We separately select nine optimized resist thicknesses from the resist thickness ranges in the absence and presence of BARC to simulate their development and extract their profile images. The results are shown in Fig. 6. Figure 6(a) shows the profile images of the resist thickness ranging from 0.11 μm to 0.13 μm in steps of 0.0025 μm in the absence of BARC, and figure 6(b) displays the profile images of the resist thickness ranging from 0.15 μm to 0.17 μm in steps of 0.0025 μm in the presence of BARC. For profile images 1–9 in Figs. 6(a) and 6(b) their resist thicknesses increase sequentially in steps of 0.0025 μm. As shown in Fig. 6(a), the CD linewidth changes a lot with resist thickness increasing in the absence of BARC. Also,

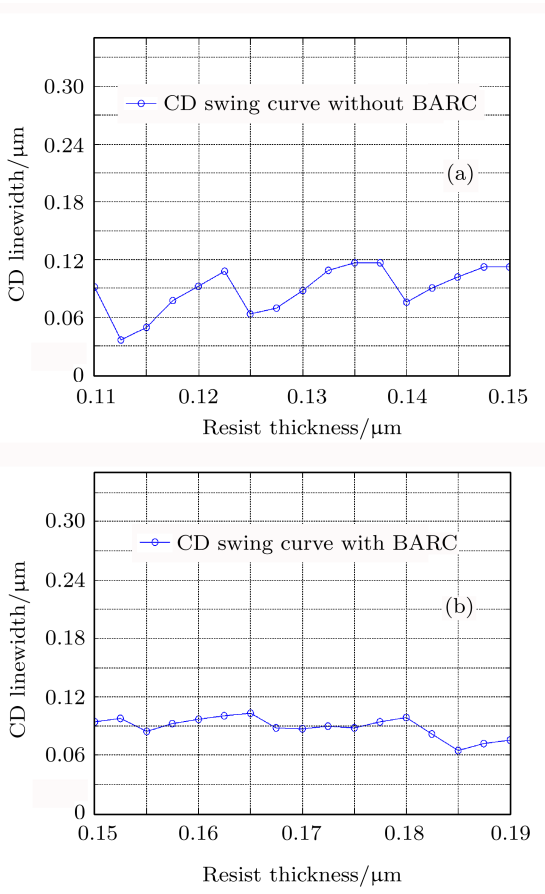


Fig. 5. Swing curves of 90-nm CD linewidth versus resist thickness in the absence (a) and presence (b) of BARC.

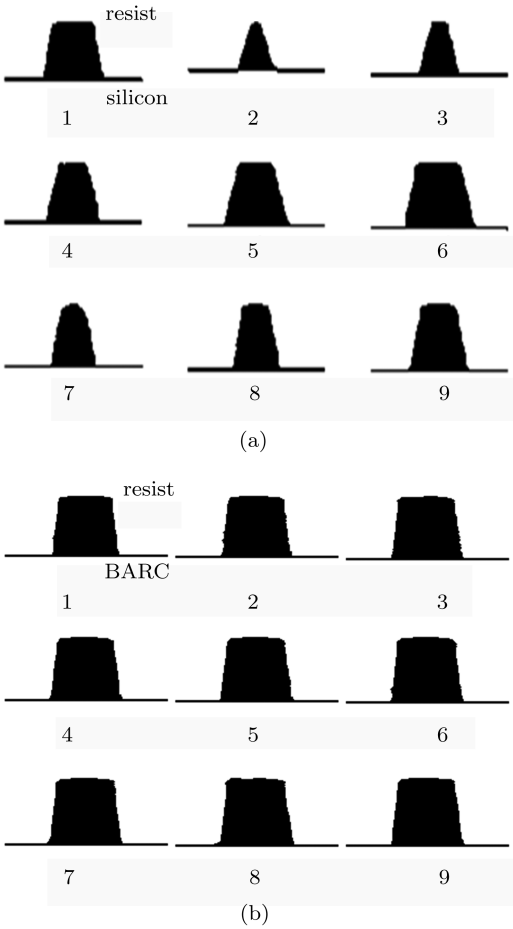


Fig. 6. Simulated CD profile images in the absence (a) and presence (b) of BARC.

of the CD linewidth in the absence of BARC becomes bigger and exceeds 10%, but the swing amplitude of it can be found from Fig. 6(a) that the sidewall effect is very obvious in the absence of BARC, and the

sidewall effect has an adverse effect on the etching technics. On the contrary, in Fig. 6(b), the CD has better profile images and changes little with the resist thickness increasing in the presence of BARC; and the sidewall effect is not obvious.

4. Conclusions

As for the ArF laser lithography system for 90-nm CD manufacturing, the accurate CD linewidth is hard to obtain with the silicon substrate because of the big reflectivity and the big swing amplitude. So, the BARC coating must be needed, and the BARC coating can effectively reduce the swing curve effect of the reflectivity and CD linewidth. The optimal resist thickness for 90-nm CD of the simulation lithography system, whose parameters are given in Table 1, is obtained to be in a range from 0.15 μm to 0.18 μm in the presence of BARC. Using simulation of the lithography process can reduce the cost and time in a wafer experiment. In practical lithography, the further optimized resist thickness can be found through a few wafer experiments in the range obtained by simulation.

References

[1] Zhang W T, Zhu B H, Huang J and Xiong X M 2011 *Acta Phys. Sin.* **60** 103203 (in Chinese)

[2] Ma B, Ma Y, Zhao M, Ma S S and Wang Z S 2006 *Acta Phys. Sin.* **55** 667 (in Chinese)

[3] Zhang W T, Zhu B H and Xiong X M 2009 *Acta Phys. Sin.* **58** 8199 (in Chinese)

[4] Korka J E 1970 *Appl. Opt.* **9** 969

[5] Mack C A 1986 *Appl. Opt.* **25** 1958

[6] Brunner T A 1991 *SPIE* **1466** 297

[7] Tanaka T, Hasegawa N, Shiraishi H and Okazaki S 1990 *J. Electrochem. Soc.* **137** 3900

[8] André S and Patrick S 2000 *Opt. Eng.* **39**776

[9] Dijkstra H J and Juffermans C 1993 *SPIE* **1927** 275

[10] Dammel R R and Norwood R A 1996 *SPIE* **2724** 754

[11] Miura S S, Lyons C F and Brunner T A 1992 *SPIE* **1674** 147

[12] Ahrens R G and Tennant D M 1999 *Microelectronic Engineering* **35 229**

[13] Hopkins H H 1957 *J. Opt. Soc. Am.* **47** 508

[14] Hopkins H H 1953 *Proc. R. Soc. Lond.* A **217** 408

[15] Dill F H, Neureuther A R and Tuttle J A 1975 *IEEE Trans. Electron Dev.* **22** 456

[16] Bernard D A 1987 *Phillips Journal of Research* **42** 566

[17] Mack C A 1985 *SPIE* **538** 207

[18] Mack C 2007 *Fundamental Principles of Optical Lithography: The Science of Microfabrication* (West Sussex: Jhon Wiley & Sons. Ltd) p. 133

[19] Ioannis K 2000 *IEEE Transactions on Semiconductor Manufacturing* **13** 61

[20] Mack C 2007 *Fundamental Principles of Optical Lithography: The Science of Microfabrication* (West Sussex: Jhon Wiley & Sons. Ltd) p. 146